3D time-dependent receiver extension for FWI

M. Benziane[1], R. Brossier[1], L. Métivier[1,2]

[1] Univ. Grenoble Alpes ISTerre; [2] Univ. Grenoble Alpes CNRS LJK

Summary

Full waveform inversion suffers from premature convergence to non-informative minima when the initial model is not accurate enough. Extension strategies rely on introducing additional degrees of freedom to the FWI problem, which makes it possible to fit the observed and the synthetic data in a wrong velocity model. This search space extension mitigates the cycle-skipping issue. Receiver extension introduces the receiver positions as a free parameter to the FWI problem. This additional freedom makes it possible to fit data when the model estimate is poor, circumventing cycle-skipping. To handle complex multi-arrival data, our receiver extension strategy uses a time-dependent relocalization approach: the receiver position depends on the acquisition time. This method is directly applicable to time-domain FWI. In this work, we extend our method to 3D using a parsimonious relocalization strategy, which consists in moving the receiver along a one dimensional direction defined by the source and receiver locations. This parsimonious relocalization strategy efficiently mitigates cycle skipping generated by a crude initial model, while maintaining an affordable computational cost. This is illustrated on a synthetic case study based on a modified 3D Overthrust model.

3D time-dependent receiver extension for FWI

Introduction

Seismic Full Waveform Inversion (FWI) is a high resolution subsurface parameters estimation method. It is formulated as a PDE constrained optimization problem, where the fit between the observed and calculated data is improved, by iteratively updating a given initial subsurface model. FWI is prone to converge to non-informative local minima. This occurs when the initial model is not accurate enough, to match the phases of the calculated and observed data within half the dominant period (Virieux and Operto, 2009). This is the well known cycle-skipping issue. Numerous strategies have been developed over the years to mitigate cycle-skipping, the review of which is beyond the scope of this study. We focus on a class of methods which enriches the search space to alleviate cycle-skipping. This search space extension makes it possible to fit the data when the model estimate is poor. Extension can be performed by introducing additional degrees of freedom in the model (Chauris and Cocher, 2017), the source (or wavefield) (Operto et al., 2023) or receivers (Métivier and Brossier, 2022), to cite a few. We focus on the latter for its straightforward application to time-domain FWI. Using this strategy, the kinematic error of the initial velocity model is compensated by a virtual receiver repositioning. Along the FWI iterations, this virtual receiver relocalization is forced to the true receiver position. To handle complex multi-arrival data, we have extended this strategy by making the receiver position time-dependent for 2D FWI (Benziane et al., 2024). In the present study, we extend our method to 3D FWI, using a parsimonious relocalization strategy. We test our method using a modified version of Overthrust 3D model (Aminzadeh et al., 1997).

Background

We write the extended-receiver FWI misfit problem as

$$\min_{m,\Delta x(t)} f(m,\Delta x(t)) \triangleq \min_{m,\Delta x(t)} \frac{1}{2}\sum_{s=1}^{N_s}\sum_{r=1}^{N_r} ||d_{cal,s}[m,\Delta x_{s,r}(t)](\mathbf{x}_r,t) - d_{obs,s}(\mathbf{x}_r,t)||_2^2 + \alpha\mathscr{P}_1[\Delta x_{s,r}(t)] + \beta\mathscr{P}_2[\Delta \dot{x}_{s,r}(t)(t)]. \tag{1}$$

The misfit function in equation 1 is bivariate, m being the model subsurface parameters, and $\Delta x(t)$ being the time-dependent receiver relocalization. r and s are the receiver and the source indices, respectively, with N_s being the number of sources, and N_r being the number of receivers. $d_{obs,s}$ are the observed data, and $d_{cal,s}[m,\Delta x_{s,r}(t)](\mathbf{x}_r,t)$ are the extended calculated data, which are extracted from the synthetic wavefield at extended receiver positions. The synthetic wavefield is computed using a wave equation

$$\begin{cases} A(m)u_s(\mathbf{x},t) = b_s(\mathbf{x},t) \\ d_{cal,s}[m](\mathbf{x}_r,t) = (R_{s,r}u_s)[m,\Delta x_{s,r}(t)](\mathbf{x},t), \end{cases} \tag{2}$$

where $A(m)$ is the wave equation operator, $u_s(\mathbf{x},t)$ is the calculated wavefield and $b_s(\mathbf{x},t)$ is the source term. The calculated data are extracted from the calculated wavefield at extended receiver positions using the restriction operator $R_{s,r}$, which is defined as a convolution with a Dirac delta function as follows

$$(R_{s,r}u_s)[m,\Delta x_{s,r}(t)](\mathbf{x},t) = \int_\Omega \delta(\mathbf{x} - (\mathbf{x}_r + \Delta x_{s,r}(t)))u_s[m](\mathbf{x},t)d\mathbf{x}. \tag{3}$$

The second and third terms ($\mathscr{P}_1$ and $\mathscr{P}_2$) on the right hand side of equation 1 are penalty terms for the receiver position and speed, respectively, with α and β being user defined tuning parameters. The time-dependent receiver relocalization is parametrized using a polynomial representation

$$\Delta x(t) = \sum_{j=1}^{n_s}\sum_{k=1}^{N_\ell} a_{k+N_\ell\times(j-1)}\ell_k^{N_\ell}(t), \tag{4}$$

where $\ell_k^{N_\ell}(t)$ are Lagrange basis functions of order N_ℓ, n_s is the number of segments and a_i ($i = k + N_\ell \times (j-1)$) are the values at the control points. The unknowns for this subproblem are therefore $a = (a_1, a_2, .., a_{N_\ell\times n_s+1})^T$, and our bivariate problem 1 can be rewritten as

$$\min_{m,a} f(m,a). \tag{5}$$

The minimization in equation 5 is performed using nested-loops optimization, where the outer loop is the conventional FWI loop which updates the subsurface parameters m, and the inner loop obtains the a_i values which define the time-dependent receiver relocalization using Particle Swarm Optimization (Kennedy and Eberhart, 1995).

The method has been developed for 2D FWI so far (Benziane et al., 2024). In this work, we extend it to 3D.

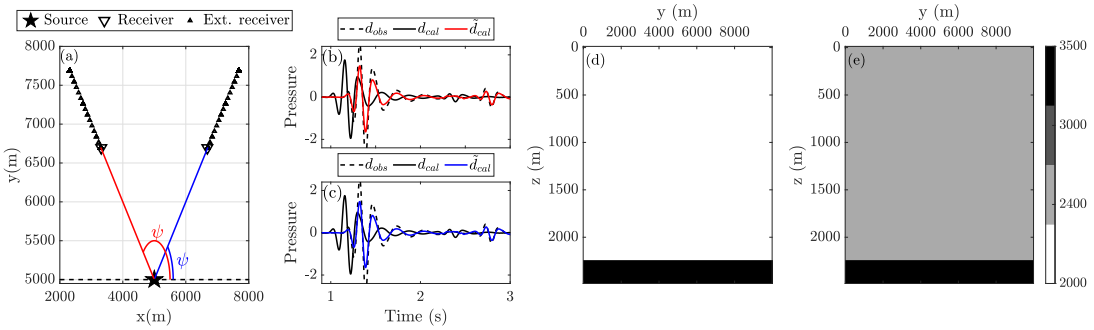

Figure 1: *3D relocalization approach illustration. (a): Relocalization following a fixed angle shown for one source and two receivers. The source is shown as a black star, the receivers as black inverted triangles, and the extended receiver positions as black triangles. (b,c): The data fit, observed data shown in a black dashed line, the calculated in a black solid line and the extended in (b) red and (c) blue, (d): a cross-section of the true model, (e): a cross-section of the initial mode. Note that the models are invariant in x.*

Parsimonious relocalization

A straightforward extension would require the use of 2D Lagrange polynomials allowing the receivers to move freely in the (x,y) plane. This would significantly increase the number of control points compared with our previous 2D FWI implementation. We thus consider an alternative parametrization strategy. Instead of allowing the receiver to move in the whole 2D plane, we restrain its motion along a 1D line connecting the receiver to the source, which we obtain from the actual positions of the source and the receiver. This formulation allows us to use the same parametrization and optimization as in the 2D case. To illustrate this strategy, we show a simple numerical experiment using one layer over a half-space (Figure 1). The true velocity is 2000 m.s^{-1} in the top layer and 3500 m.s^{-1} in the half-space. The starting velocity is set to 2400 m.s^{-1} in the top layer, we keep the true velocity in the half-space. The observed data are shown in a black dashed line, the synthetic in a black solid line, and the extended calculated data in red and blue. The receiver moves as a function of the acquisition time to fit the transmitted and reflected arrivals, the positions occupied by the extended receivers at given acquisition times are shown as black triangles. Allowing the receiver to move following the direction defined by the source and receiver positions, makes it possible to obtain a fit in the wrong velocity model. We support our parsimonious relocalization strategy with a simple numerical experiment (Figure 2). In the same medium, we consider a single source/receiver couple, we perform the relocalization following a single angle, scanning for 360 angles between $[-\pi, \pi]$, obtaining an optimal relocalization for each angle. We plot the optimal positions obtained for each angle, where the color scale indicates the misfit function value. Since the receiver position depends on the acquisition time, the plot shows different receiver positions, which are occupied by the extended receiver at given simulation times. The lowest cost values are achieved by moving the receiver following angles close to the angle defined by the source and receiver positions (dark blue color in Figure 2). Therefore, receiver relocalization following a fixed angle, defined by the source and receiver positions, appears to be sufficient.

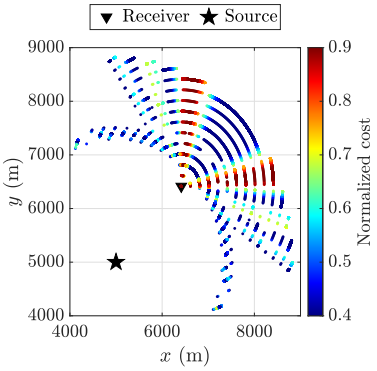

Figure 2: *A numerical experiment to support our parsimonious relocalization strategy. For a single receiver, we perform the inner loop optimization for various angles around the receiver. Each point correspond to time-dependent extended receiver positions, the color map corresponds to the misfit function value.*

Numerical example using the Overthrust model

We test our method using a modified 3D Overthrust model (Aminzadeh et al., 1997). We modify it by adding a water layer, and reducing the contrast at the seafloor to mimic marine environments. We generate the observed data using the model shown in Figure 3a, under the acoustic approximation. The acquisition contains 1024 sources, with 620 m spacing and x-line spacing. As for the receivers, we use 17161 receivers with 150 m spacing and in-line spacing. For the inversion, we use random source sub-sampling (Warner et al., 2013). We perform 3 l-BFGS iterations (Nocedal and Wright, 2006) for each group of 192 shots, for a total of 113 iterations of extended receiver FWI and conventional FWI. The inversion is performed in the 2-5 Hz frequency band. The initial model is obtained by Gaussian smoothing of the true model, with a correlation length of 4500 m.

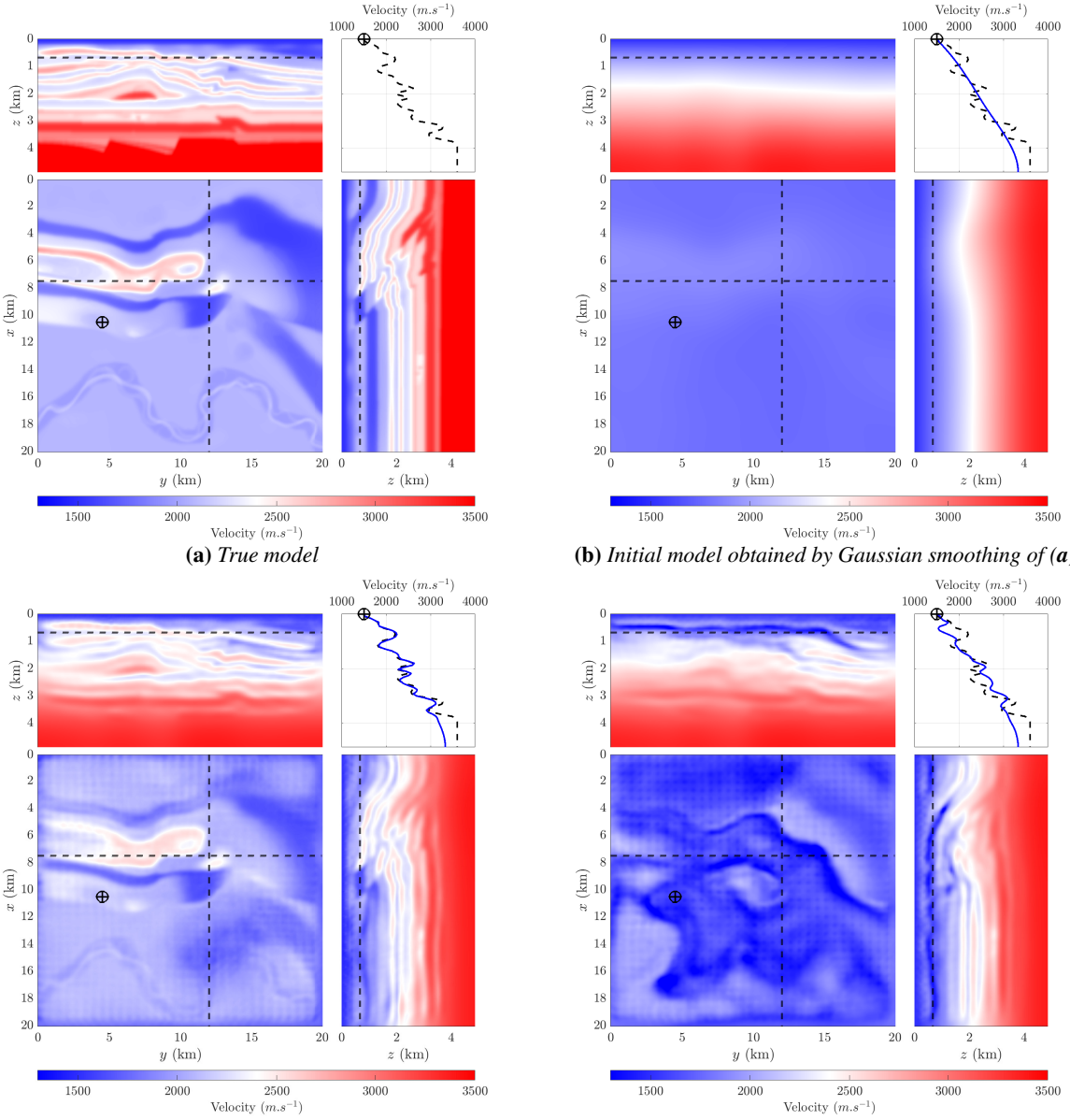

(a) *True model*

(b) *Initial model obtained by Gaussian smoothing of (a)*

(c) *Reconstructed model obtained using receiver extension*

(d) *Reconstructed model obtained using conventional FWI*

Figure 3: *Numerical experiment using the Overthrust model. The $\bigoplus$ symbol indicates the location where 1D velocity profiles are extracted, which are shown in the top right panel of each figure, the black dashed line corresponds to the true model.*

Conventional FWI fails to reconstruct the velocity model from this crude initial model, which is the result of cycle-skipping. Extended-receiver FWI velocity model estimation is satisfactory. We are able to reconstruct the different features of the Overthrust model, which is clear in Figure 3c. We note that the method struggles to retrieve the correct velocity in the region around $x = 15$ km and $y = 12$ km. We show a x-z section trough this region, where the flat low velocity layer deflects upwards. Nonetheless, these preliminary results are very satisfactory and warrant further investigation. We extract a 1D velocity profile, which are shown in the top right panel of each figure. The reconstruction is satisfactory for depths down to 2 km. In the lower part of the model, the velocity estimation follows the trend of the true model. Receiver-extension is able to circumvent cycle-skipping by explaining the data when the model estimate is poor.

To better illustrate how the time-dependent receiver extension works in practice, we show the observed wavefield, the synthetic wavefield and the extended wavefield at receivers locations (at the surface). The synthetic wavefield is computed in the initial model (Figure 3b). The extended wavefield is obtained by allowing the receivers to move as a function of the acquisition time, as such, the data extraction from the 3D synthetic wavefield is performed at extended receiver locations (equation 3), not the actual receivers positions.

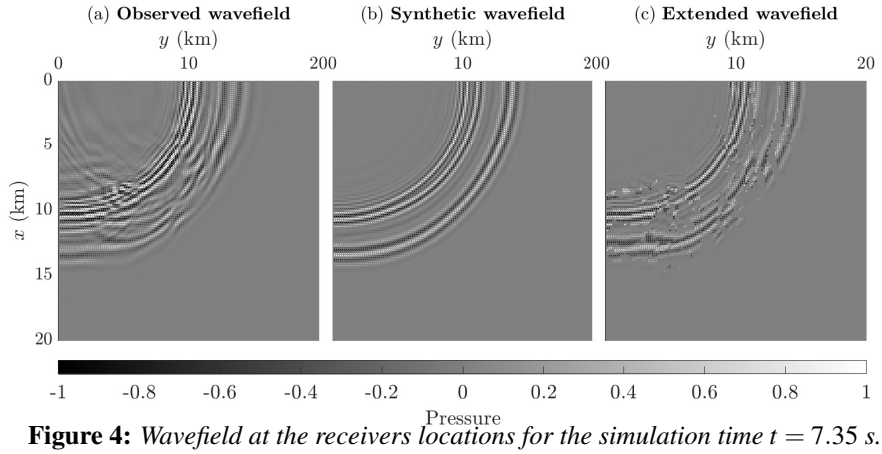

Figure 4: *Wavefield at the receivers locations for the simulation time $t = 7.35$ s.*

The synthetic wavefield (Figure 4b) corresponds to the conventional FWI, where it is simply extracted from the 3D synthetic wavefield at the actual receivers locations. This synthetic wavefield does not match the observed wavefield, causing conventional FWI to converge to a spurious minimum. The extended wavefield on the other hand, resembles –to some extent– the observed one. Our parsimonious relocalization strategy is able to satisfactorily match the wavefield at the surface, in a difficult initial model, circumventing cycle-skipping. Interestingly enough, this 2D view of the receiver extended wavefield is reminiscent of the extended wavefield obtained in the frame of Wavefield Reconstruction Inversion (WRI), an alternative extension strategy where the additional degree of freedom is defined at the wavefield level. In WRI, the extended wavefield is obtained –everywhere– so as to simultaneously fit the data and the wave equation in the least-squares sense. Such methods have shown to be very powerful against cycle skipping however their usage for time-domain FWI is not straightforward (Operto et al., 2023).

Conclusion and perspectives

We show that receiver extension can be extended to 3D. Our implementation relies on a parsimonious relocalization strategy, which appears to be sufficient to mitigate cycle skipping on a 3D realistic synthetic example, while maintaining an affordable computational complexity. Our preliminary results are promising, which encourages further investigation. The next step is application to a real industry dataset.

Acknowledgements

This study was partially funded by the SEISCOPE consortium (*http://seiscope2.osug.fr*), sponsored by AKERBP, DUG, EXXONMOBIL, GEOLINKS, JGI, PETROBRAS, SHELL, SINOPEC, TOTALENERGIES and VIRIDIEN. This study was granted access to the HPC resources provided by the GRICAD infrastructure (https://gricad.univ-grenoble-alpes.fr), which is supported by Grenoble research communities, the HPC resources of Cray Marketing Partner Network (`https://partners.cray.com`), and those of CINES/IDRIS/TGCC under the allocation 046091 made by GENCI.

References

Aminzadeh, F., Brac, J. and Kunz, T. [1997] *3-D Salt and Overthrust models*. SEG/EAGE 3-D Modeling Series No.1.

Benziane, M., Brossier, R., Métivier, L. and Sambolian, S. [2024] Full-waveform inversion with time-dependent receiver-extension: An efficient inner loop optimization. In: *Fourth International Meeting for Applied Geoscience & Energy*. 1038–1042.

Chauris, H. and Cocher, E. [2017] From migration to inversion velocity analysis. *Geophysics*, **82**(3), S207–S223.

Kennedy, J. and Eberhart, R. [1995] Particle swarm optimization. In: *Proceedings of ICNN'95 - International Conference on Neural Networks*, 4. 1942–1948 vol.4.

Métivier, L. and Brossier, R. [2022] Receiver-extension strategy for time-domain full-waveform inversion using a relocalization approach. *Geophysics*, **87**(1), R13–R33.

Nocedal, J. and Wright, S.J. [2006] *Numerical Optimization*. Springer, 2nd edn.

Operto, S., Gholami, A., Aghamiry, H., Guo, G., Beller, S., Aghazade, K., Mamfoumbi, F., Combe, L. and Ribodetti, A. [2023] Extending the search space of full-waveform inversion beyond the single-scattering Born approximation: A tutorial review. *GEOPHYSICS*, **88**(6), R671–R702.

Virieux, J. and Operto, S. [2009] An overview of full waveform inversion in exploration geophysics. *Geophysics*, **74**(6), WCC1–WCC26.

Warner, M., Ratcliffe, A., Nangoo, T., Morgan, J., Umpleby, A., Shah, N., Vinje, V., Stekl, I., Guasch, L., Win, C., Conroy, G. and Bertrand, A. [2013] Anisotropic 3D full-waveform inversion. *Geophysics*, **78**(2), R59–R80.